



Cite this: *Polym. Chem.*, 2016, 7, 5996

## Dual-responsive supramolecular colloidal microcapsules from cucurbit[8]uril molecular recognition in microfluidic droplets†

Ziyi Yu,<sup>‡a</sup> Yang Lan,<sup>‡b,c</sup> Richard M. Parker,<sup>a</sup> Wangqing Zhang,<sup>c</sup> Xu Deng,<sup>d</sup> Oren A. Scherman<sup>\*b</sup> and Chris Abell<sup>\*a</sup>

The macrocyclic host, cucurbit[8]uril, is used to facilitate cross-linking of colloidal particles and polymers in microdroplets resulting in thermo- and photo-responsive supramolecular colloidal microcapsules. Methyl viologen-bearing colloidal particles were prepared using template polymerisation and combined with cucurbit[8]uril and an azobenzene-functionalised polymer within microfluidic droplets. The colloidal particles self-assembled at the droplet interface, whereupon polymeric cross-links formed *via* ternary host-guest complexation with cucurbit[8]uril. The resultant supramolecular colloidal microcapsules were uniform in size and were able to retain a macromolecular cargo. It is shown that the capsule skin porosity, and consequently the rate of release of encapsulated cargo, can be remotely controlled *via* either temperature or light triggers. This simple and versatile method could be extended to other polymer or colloidal derivatives for the fabrication of nano- and microcapsules with dual stimuli response for controlled release.

Received 6th July 2016,  
Accepted 2nd September 2016

DOI: 10.1039/c6py01171c

www.rsc.org/polymers

### Introduction

Organisms owe their unique and diverse structures in part to selective molecular recognition by biomolecules, such as DNA–proteins, sugar–lectins, RNA–ribosomes, *etc.*<sup>1–3</sup> Since the first example of crown ether reported to mimic this process,<sup>4</sup> a number of artificial molecular recognition systems have been established.<sup>5–9</sup> For example, cyclodextrins (CDs) are employed as macrocyclic hosts for the construction of supramolecular structures *via* specific binding within their hydrophobic cavities.<sup>10,11</sup> Relying on a concerted set of weak interactions, cup-like calix[*n*]arenes act as receptors to hold monomer units together to enable calixarene-based supramolecular polymerisation.<sup>12</sup> Driven by the hydrogen bonds or hydrophobic and ion pair interactions, supramolecular polymers can be efficiently constructed by pillar[*n*]arenes and their complementary molecules.<sup>13,14</sup> On account of the dynamic and reversible char-

acter of non-covalent interactions in molecular recognition systems, such supramolecular structures undergo dynamic assembly and disassembly processes under external stimuli. Thereby, supramolecular materials are capable of adapting to their environment and exhibit a wide variety of attractive ‘smart’ properties including shape-memory, self-healing, and stimuli-responsivity.<sup>15–20</sup>

Recently, the family of cucurbit[*n*]urils (CB[*n*], *n* = 5–8, 10) and their corresponding guest molecules have attracted considerable attention as molecular recognition systems, due to their exceptionally high equilibrium affinities and their outstanding stimuli responsively properties.<sup>21–26</sup> CB[*n*] molecules are cyclic, methylene-linked oligomers of glycoluril, having a symmetric ‘barrel’ shape with two identical portal regions laced by ureido-carbonyl oxygens. The size of the ‘molecular container’ is determined by the number of glycoluril units. While CB[5], CB[6], and CB[7] are all able to bind single guests, such as cationic amines, metals, or imidazolium ions, CB[8] has a larger cavity volume and can simultaneously accommodate up to two guest molecules. Typically, these comprise an electron-deficient first guest (*e.g.* methyl viologen) and an electron-rich second guest (*e.g.* naphthalene or azobenzene) to form a stable 1 : 1 : 1 heteroternary supramolecular complex.

Previous research has demonstrated that the utility of CB[8] as a linking agent to enable guest-functionalised polymers to be reversibly complexed into supramolecular cross-linked materials.<sup>27–29</sup> Furthermore, we have previously reported the

<sup>a</sup>Department of Chemistry, University of Cambridge, Lensfield Road, Cambridge CB2 1EW, UK. E-mail: ca26@cam.ac.uk

<sup>b</sup>Melville Laboratory for Polymer Synthesis, Department of Chemistry, University of Cambridge, Lensfield Road, Cambridge CB2 1EW, UK. E-mail: oas23@cam.ac.uk

<sup>c</sup>Collaborative Innovation Center of Chemical Science and Engineering (Tianjin), Institute of Polymer Chemistry, Nankai University, Tianjin 300071, China

<sup>d</sup>Institute of Fundamental and Frontier Sciences, University of Electronic Science and Technology of China, Chengdu 610054, China

†Electronic supplementary information (ESI) available. See DOI: 10.1039/c6py01171c

‡These authors contributed equally to this work.





XL-01-171 fluorosurfactant ( $200 \mu\text{L h}^{-1}$ ). Upon intersection the aqueous stream was segmented into monodisperse W/O microdroplets that were passed through a winding channel to allow rapid and thorough mixing of the reagents prior to collection. As each CB[8] cavity can accommodate one pair of guests, the concentration of the stock solutions was prepared such that the ratio of MV:CB[8]:azobenzene within the mixed droplet was equimolar ( $40 \times 10^{-6} \text{ M}$ ). It should be noted that this concentration is too low to allow significant complexation to occur within the droplet, but when MV, CB[8], and azobenzene accumulate at the interface, the concentration is high enough to form a supramolecular shell.

As shown in Fig. 3a, the stable microdroplets exhibit a high level of monodispersity, as indicated by the narrow size distribution with a mean diameter of  $62 \mu\text{m}$  and a low coefficient of variation of 2%. The distribution of the capsule-forming components within the microdroplets was probed by confocal laser scanning fluorescence microscopy (CLSM), utilising the Rhodamine B-labeled variant of AP. The CLSM image of microdroplets in Fig. 3a shows the red fluorescence from AP is localised (and concentrated) at the spherical interface of the microdroplet, templating the formation of a hollow colloidal microcapsule shell.

Evaporation of water from the microdroplets results in a steady decrease in diameter until cross-linking at the interface is sufficient for a robust supramolecular shell to form. Further evaporation leads to buckling and crumpling of the flexible shell, until eventual complete collapse onto the glass substrate (Fig. 4a). The morphology of the obtained microcapsules was further investigated by scanning electron microscopy (SEM); Fig. 4b shows that in contrast to solid beads, microcapsules collapse upon dehydration because of the lack of internal

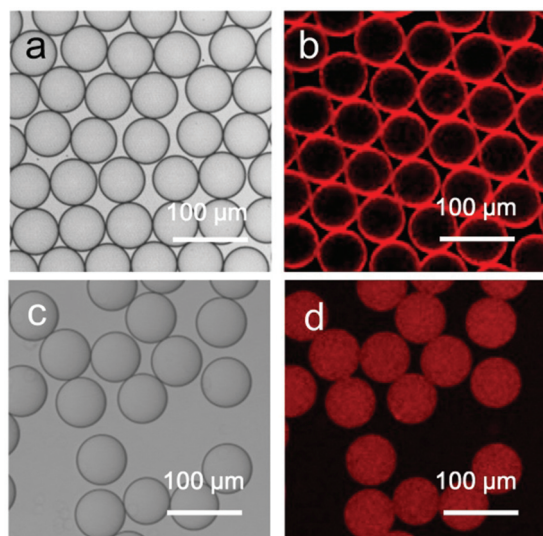


**Fig. 3** Optical and confocal laser scanning microscopy (CLSM) images of (a–b) microdroplets containing capsule-forming components: MCP, Rhodamine B-labelled AP, and CB[8] and (c–d) control experiments with microdroplets exclusively containing Rhodamine B-labelled AP.

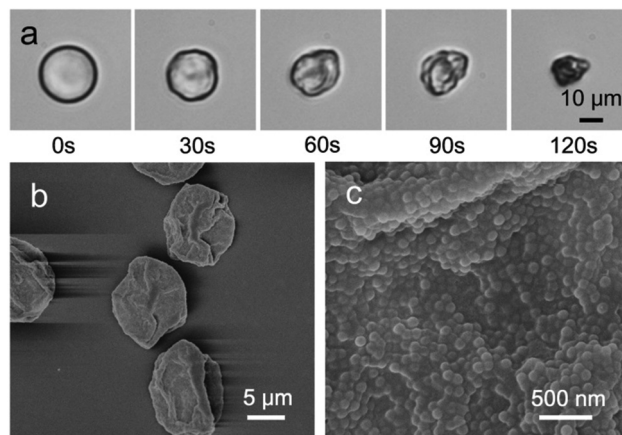


**Fig. 4** (a) Micrographs of the final stages of the evaporative microcapsule formation process, resulting in a collapsed structure. (b–c) Scanning electron microscope (SEM) images of dry microcapsules.

support, with creases and folds clearly visible on the surface. The skin of the microcapsules is constructed from a composite network of colloidal particles (MCP) within a polymer matrix (AP), as shown in an enlarged SEM image (Fig. 4c), where closely-packed colloidal particles are observed. The high degree of monodispersity of the microdroplet template results in the isolation of stable supramolecular microcapsules of uniform size (Fig. S7, ESI†).

### The driving force of formation

Colloidal particles owe their stabilizing effect at a liquid–liquid interface to high attachment energies. This effect is employed in the formation of the colloidosome microarchitecture.<sup>36–38</sup> Consequentially, it can be postulated that MCP-CB[8] colloids self-assemble at the droplet interface to form a Pickering-stabilised emulsion.

This accumulation not only results in a localised enhancement in concentration, but also synergistically (*via* CB[8] cross-links) adsorbs AP at the boundary of the microdroplet to form a supramolecular nanocomposite skin. To illustrate this, W/O microdroplets exclusively containing the Rhodamine B-labelled variant of AP were prepared and imaged by CLSM (Fig. 3c and d). In contrast with droplets containing the MCP-CB[8]-CAP ternary complex (Fig. 3a and b), the fluorescence from AP is uniformly distributed across the entire volume of the droplets rather than locating at the interfaces. This negative control experiment highlights the requirement for MCP colloids and CB[8] to direct self-assembly towards a hollow, microcapsule structure.

### Encapsulation of cargo

The segregation of the aqueous flow into discrete microdroplets in the device enables the microcapsules to be loaded with a water-soluble cargo in a single step. To demonstrate this, fluorescein isothiocyanate-dextran (FD,  $0.1 \text{ mg mL}^{-1}$ ,  $M_w = 150 \text{ kDa}$ ) was mixed in bulk with Rhodamine B-labelled



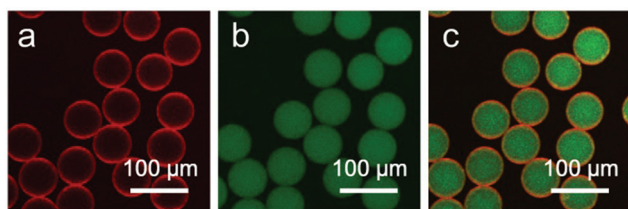


**Fig. 5** CLSM images of microdroplets encapsulating fluorescein isothiocyanate-dextran cargo and capsule-forming components: MCP, AP and CB[8]. (a) Red channel: Rhodamine B-labelled AP, (b) green channel: FD and (c) overlaid.

variant of **AP** and the colloidal microcapsules were prepared as described above. CLSM images of the resultant microdroplets are shown in Fig. 5. Red fluorescence from Rhodamine B can be clearly resolved at the oil/water interface, while green fluorescence from the **FD** cargo is dispersed throughout the interior of the droplets. Note that the assembly of the **MCP**CB[8]**CAP** supramolecular layer is not disrupted by the presence of the aqueous cargo.

The cargo-loaded supramolecular colloidal microcapsules can be dehydrated and subsequently rehydrated in water, where they were observed to swell (Fig. 6a[1–3]). Osmotic

pressure, arising from the presence of the macromolecular cargo, results in the microcapsule diameter increasing on average by 1.5× compared to the dry capsule. Furthermore, the folds and creases diminish, and it is possible to see the top and the lower layers of the microcapsule are still distinct. Despite being constructed exclusively from water-soluble components, the strength of the CB[8]-based ternary complex ( $K_a$  up to  $10^{12} \text{ M}^{-2}$  in water)<sup>39</sup> endows high stability.

To assess the significance of the role of the CB[8] host-guest network in cargo retention, a number of control experiments were carried out. As illustrated in Fig. 6, **MCP**CB[8]**CAP** supramolecular colloidal microcapsules can retain 150 kDa FD when rehydrated in water. In contrast, the self-assembly of **MCP** colloids to form a colloidal shell is alone not sufficient to retain **FD** upon hydration, with fluorescence observed in the surrounding media. Similarly, encapsulation of **FD** was not observed when the experiment was performed with only hydrophilic polymer **AP** present in the microdroplet. Finally, mixing **MCP** and **AP**, but in the absence of CB[8], does not offer any significant improvement in efficacy over **MCP** alone.

### Dual-responsive properties of the supramolecular microcapsules

With the inclusion of the thermo-responsive NIPAM moiety within the outer shell of **MCP**, the molecular permeability of the microcapsule and correspondingly the release rate of encapsulated cargo can be controlled. To test the temperature dependence of the permeability of rehydrated supramolecular microcapsules, 150 kDa FD was loaded as before and then the release of cargo upon rehydration tracked at three different temperatures: 25, 35 and 45 °C (Fig. 7). As the temperature increased, the rate of FD dispersal from the microcapsules also increased; with only 28% of cargo released over the first 30 minutes at 25 °C, but 55% of cargo released over the same time period on raising the temperature to 45 °C.

This temperature-induced cargo release behaviour is attributed to the thermo-responsive PNIPAM shell of **MCP**, which collapses upon increasing the temperature above the lower critical solution temperature (LCST). This introduces larger

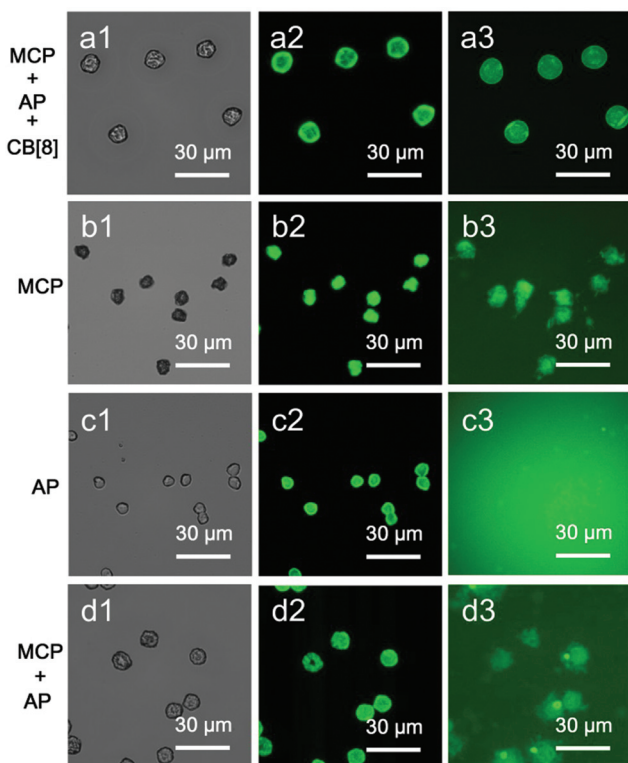


**Fig. 6** (a1) Optical and (a2) fluorescence micrographs of dried supramolecular microcapsules loaded with FD (150 kDa), and (a3) after rehydration in water for 5 minutes. This is compared with microstructures prepared from microdroplets containing (b1–b3) only the MCP component, (c1–c3) only AP component, and (d1–d3) MCP and AP components in the absence of CB[8].

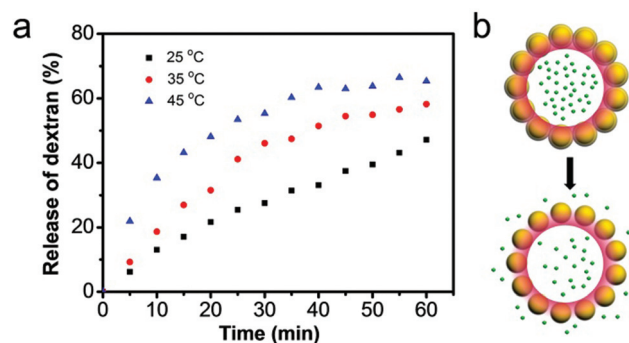


**Fig. 7** (a) The release profiles of 150 kDa FD cargo from microcapsules over 1 h, at temperatures: 25, 35 and 45 °C. (b) Schematic representation of the contraction of the colloidal particles upon increasing temperature, resulting in release of encapsulated cargo.



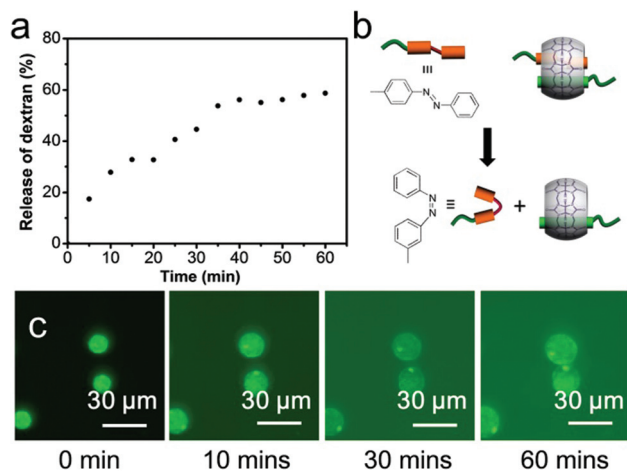


**Fig. 8** (a) The release profile of 150 kDa FD cargo from microcapsules over 1 h after 30 s of UV irradiation at 377 nm. (b) Schematic representation of the photochemical disassembly of the ternary complex between MV, azobenzene, and CB[8]. (c) Fluorescence images showing the triggered release of 150 kDa FD cargo from microcapsules, upon exposure to UV light.

gaps between colloidal particles, resulting in the formation of larger pores (Fig. 7b).

Beyond offering a means for locking colloids and polymer together, the supramolecular CB[8] cross-link can also be employed to trigger the release of encapsulated cargo. Here, azobenzene was selected as the second guest, as its inclusion within CB[8] can be switched on or off by photoisomerisation from the *trans*- to the *cis*-isomer, as illustrated in Fig. 8b. To investigate the efficacy of photo-triggered cargo release, 150 kDa FD-loaded microcapsules were rehydrated in water at 25 °C and then exposed to UV light (30 s,  $\lambda_{\text{max}} = 377$  nm). Fig. 8a shows the release profile for microcapsules loaded with FD as a function of the time, post UV-exposure. Compared to Fig. 7, after 5 min the extent of cargo release from UV-irradiated microcapsules was three times greater. To release 50% of their original FITC-dextran, the microcapsules took 30 min after UV irradiation compared with 60 min in the absence of UV. It should be noted that photo-isomerisation of the azobenzene moiety does not lead to complete disassembly, with a photostationary state 80% *cis*-in the presence of CB[8].<sup>40</sup> UV exposure results in an expansion of the microcapsule diameter rather than complete disassembly, with a corresponding increase in permeability (Fig. 8c).

## Conclusion

By combining CB[8]-based host-guest recognition with the self-assembly of colloidal particles within microfluidic droplets, dual-responsive colloidal supramolecular microcapsules were prepared. The resultant microcapsules offer good monodispersity and facile release *via* the supramolecular cross-links. Moreover, it was shown that the release of cargo from supra-

molecular colloidal microcapsules can be achieved by changing the porosity of the supramolecular membrane under mild conditions, using temperature or UV light. The high degree of customization enabled by our bottom-up assembly approach, combined with the simplicity of microdroplet fabrication allows ready access to a wide range of microencapsulation motifs.

## Experimental

### Materials and equipment

All starting materials were purchased from Alfa Aesar or Sigma Aldrich and used as received, unless stated otherwise. CB[8] was prepared as documented previously.<sup>41,42</sup> 400 MHz <sup>1</sup>H NMR spectra were recorded using a Bruker Avance QNP 400. ATR FT-IR spectroscopy was performed using a Perkin-Elmer Spectrum 100 series FT-IR spectrometer equipped with a universal ATR sampling accessory. UV-visible absorption studies were performed on a Varian Cary 4000 UV-vis spectrophotometer. Scanning electron microscopy (SEM) measurements were made and images recorded using a Leo 1530 variable pressure SEM with InLens detector. Dynamic light scattering (DLS) measurement was performed on Malvern Zeta-sizer NS90 instrument. Images of droplet formation were obtained using a Phantom v7.2 camera attached to an Olympus IX-71 inverted microscope. Transmission and fluorescence micrographs were obtained using an Olympus IX-81 inverted optical microscope coupled with an Andor Technology EMCCD iXonEM+ DU 897 camera. Laser scanning confocal microscopy (LSCM) measurements were carried out using a Leica TCS SP5 confocal microscope. Samples were illuminated with either 488 nm or 544 nm lasers for exciting the fluorescein isothiocyanate-dextran cargo and the Rhodamine-containing azobenzene-poly(vinyl alcohol) polymer respectively. The emission of FITC-dextran, peaking at 520 nm (product data sheet) and the emission of Rhodamine B, peaking at 582 nm, were collected over emission band passes of 490–540 nm and 560–650 nm respectively.

### Synthesis of polymeric template colloidal particles of PST-*co*-PStMV

1-Methyl-1'-(4-vinylbenzyl)-[4,4'-bipyridine]-1,1'-dium chloride iodide (StMV, 0.23 g, 0.5 mmol) was dissolved in water (100 mL) to form a homogeneous solution, to which styrene (St, 5.208 g, 50.0 mmol) was added dropwise. The mixture for purged with nitrogen for 1 h before elevating the temperature, with the nitrogen blanket maintained throughout the polymerisation. After stabilizing at 80 °C, polymerisation was initiated by the addition of 2,2'-azobis(2-methylpropionamide) dihydrochloride (AIBA, 0.271 g, 1.0 mmol). The mixture was allowed to polymerise for 24 h, followed by dialysis to purify and dispersal in 100 mL water.

### Synthesis of MV-bearing colloidal particles (MCP)

The MV-bearing colloidal particles were prepared using template polymerisation. To a 250 mL flask, the dispersion of PST-





- 4 R. C. Helgeson, T. L. Tarnowski, J. M. Timko and D. J. Cram, *J. Am. Chem. Soc.*, 1977, **99**, 6411–6418.
- 5 C. Cheng, P. R. McGonigal, S. T. Schneebeli, H. Li, N. A. Vermeulen, C. Ke and J. F. Stoddart, *Nat. Nanotechnol.*, 2015, **10**, 547–553.
- 6 J. A. Krings, B. Vonhoren, P. Tegeder, V. Siozios, M. Peterlechner and B. J. Ravoo, *J. Mater. Chem. A*, 2014, **2**, 9587–9593.
- 7 K. Liu, Y. Kang, Z. Wang and X. Zhang, *Adv. Mater.*, 2013, **25**, 5530–5548.
- 8 R. Yi, G. Ye, D. Pan, F. Wu, M. Wen and J. Chen, *J. Mater. Chem. A*, 2014, **2**, 6840–6846.
- 9 G. Yu, K. Jie and F. Huang, *Chem. Rev.*, 2015, **115**, 7240–7303.
- 10 S. Dong, B. Zheng, F. Wang and F. Huang, *Acc. Chem. Res.*, 2014, **47**, 1982–1994.
- 11 A. Harada, Y. Takashima and M. Nakahata, *Acc. Chem. Res.*, 2014, **47**, 2128–2140.
- 12 D.-S. Guo and Y. Liu, *Chem. Soc. Rev.*, 2012, **41**, 5907–5921.
- 13 X.-B. Hu, L. Chen, W. Si, Y. Yu and J.-L. Hou, *Chem. Commun.*, 2011, **47**, 4694–4696.
- 14 Z. Zhang, Y. Luo, J. Chen, S. Dong, Y. Yu, Z. Ma and F. Huang, *Angew. Chem., Int. Ed.*, 2011, **123**, 1433–1437.
- 15 F. Huang and O. A. Scherman, *Chem. Soc. Rev.*, 2012, **41**, 5879–5880.
- 16 J. Boekhoven and S. I. Stupp, *Adv. Mater.*, 2014, **26**, 1642–1659.
- 17 R. Huang, S. Wu, A. Li and Z. Li, *J. Mater. Chem. A*, 2014, **2**, 1672–1676.
- 18 K. Miyamae, M. Nakahata, Y. Takashima and A. Harada, *Angew. Chem., Int. Ed.*, 2015, **54**, 8984–8987.
- 19 C. Qin, Y. Feng, W. Luo, C. Cao, W. Hu and W. Feng, *J. Mater. Chem. A*, 2015, **3**, 16453–16460.
- 20 M. Xiao, Y. Xian and F. Shi, *Angew. Chem., Int. Ed.*, 2015, **54**, 8952–8956.
- 21 Q. An, C. Dong, W. Zhu, C.-a. Tao, H. Yang, Y. Wang and G. Li, *Small*, 2012, **8**, 562–568.
- 22 H. S. El-Sheshtawy, B. S. Bassil, K. I. Assaf, U. Kortz and W. M. Nau, *J. Am. Chem. Soc.*, 2012, **134**, 19935–19941.
- 23 X.-L. Ni, X. Xiao, H. Cong, L.-L. Liang, K. Cheng, X.-J. Cheng, N.-N. Ji, Q.-J. Zhu, S.-F. Xue and Z. Tao, *Chem. Soc. Rev.*, 2013, **42**, 9480–9508.
- 24 Y. Jang, R. Natarajan, Y. H. Ko and K. Kim, *Angew. Chem., Int. Ed.*, 2014, **53**, 1003–1007.
- 25 A. E. Kaifer, *Acc. Chem. Res.*, 2014, **47**, 2160–2167.
- 26 J. Liu, C. S. Y. Tan, Y. Lan and O. A. Scherman, *Macromol. Chem. Phys.*, 2016, **217**, 319–332.
- 27 E. A. Appel, F. Biedermann, U. Rauwald, S. T. Jones, J. M. Zayed and O. A. Scherman, *J. Am. Chem. Soc.*, 2010, **132**, 14251–14260.
- 28 J. Geng, F. Biedermann, J. M. Zayed, F. Tian and O. A. Scherman, *Macromolecules*, 2011, **44**, 4276–4281.
- 29 E. A. Appel, X. J. Loh, S. T. Jones, F. Biedermann, C. A. Dreiss and O. A. Scherman, *J. Am. Chem. Soc.*, 2012, **134**, 11767–11773.
- 30 J. Zhang, R. J. Coulston, S. T. Jones, J. Geng, O. A. Scherman and C. Abell, *Science*, 2012, **335**, 690–694.
- 31 G. Stephenson, R. M. Parker, Y. Lan, Z. Yu, O. A. Scherman and C. Abell, *Chem. Commun.*, 2014, **50**, 7048–7051.
- 32 Y. Zheng, Z. Yu, R. M. Parker, Y. Wu, C. Abell and O. A. Scherman, *Nat. Commun.*, 2014, **5**, 5772.
- 33 R. M. Parker, J. Zhang, Y. Zheng, R. J. Coulston, C. A. Smith, A. R. Salmon, Z. Yu, O. A. Scherman and C. Abell, *Adv. Funct. Mater.*, 2015, **25**, 4091–4100.
- 34 Z. Yu, J. Zhang, R. J. Coulston, R. M. Parker, F. Biedermann, X. Liu, O. A. Scherman and C. Abell, *Chem. Sci.*, 2015, **6**, 4929–4933.
- 35 Z. Yu, Y. Zheng, R. M. Parker, Y. Lan, Y. Chao, R. J. Coulston, J. Zhang, O. A. Scherman and C. Abell, *ACS Appl. Mater. Interfaces*, 2016, **8**, 8811–8820.
- 36 A. D. Dinsmore, M. F. Hsu, M. G. Nikolaidis, M. Marquez, A. R. Bausch and D. A. Weitz, *Science*, 2002, **298**, 1006–1009.
- 37 B. Samanta, D. Patra, C. Subramani, Y. Ofir, G. Yesilbag, A. Sanyal and V. M. Rotello, *Small*, 2009, **5**, 685–688.
- 38 Q. Yuan, O. J. Cayre, S. Fujii, S. P. Armes, R. A. Williams and S. Biggs, *Langmuir*, 2010, **26**, 18408–18414.
- 39 E. A. Appel, J. del Barrio, X. J. Loh and O. A. Scherman, *Chem. Soc. Rev.*, 2012, **41**, 6195–6214.
- 40 J. del Barrio, P. N. Horton, D. Lairez, G. O. Lloyd, C. Toprakcioglu and O. A. Scherman, *J. Am. Chem. Soc.*, 2013, **135**, 11760–11763.
- 41 J. Kim, I.-S. Jung, S.-Y. Kim, E. Lee, J.-K. Kang, S. Sakamoto, K. Yamaguchi and K. Kim, *J. Am. Chem. Soc.*, 2000, **122**, 540–541.
- 42 A. Day, A. P. Arnold, R. J. Blanch and B. Snushall, *J. Org. Chem.*, 2001, **66**, 8094–8100.

